

Post-Hurricane Vegetative Debris Assessment Using Spectral Indices Derived from Satellite Imagery

Transportation Research Record
1–20© National Academy of Sciences:
Transportation Research Board 2021

Article reuse guidelines:

sagepub.com/journals-permissions

DOI: 10.1177/03611981211029921

journals.sagepub.com/home/trr



Alican Karaer¹ , Mehmet Baran Ulak² , Tarek Abichou¹,
Reza Arghandeh³ , and Eren Erman Ozguven¹

Abstract

Transportation systems are vulnerable to hurricanes and yet their recovery plays a critical role in returning a community to its pre-hurricane state. Vegetative debris is among the most significant causes of disruptions on transportation infrastructure. Therefore, identifying the driving factors of hurricane-caused debris generation can help clear roadways faster and improve the recovery time of infrastructure systems. Previous studies on hurricane debris assessment are generally based on field data collection, which is expensive, time consuming, and dangerous. With the availability and convenience of remote sensing powered by the simple yet accurate estimations on the vigor of vegetation or density of manufactured features, spectral indices can change the way that emergency planners prepare for and perform vegetative debris removal operations. Thus, this study proposes a data fusion framework combining multispectral satellite imagery and various vector data to evaluate post-hurricane vegetative debris with an exploratory analysis in small geographical units. Actual debris removal data were obtained from the City of Tallahassee, Florida after Hurricane Michael (2018) and aggregated into U.S. Census Block Groups along with four groups of datasets representing vegetation, storm surge, land use, and socioeconomic. Findings suggest that vegetation and other land characteristics are more determinant factors on debris generation, and Modified Soil-Adjusted Vegetation Index (MSAVI2) outperforms other vegetation indices for hurricane debris assessment. The proposed framework can help better identify equipment stack locations and temporary debris collection centers while providing resilience enhancements with a focus on the transportation infrastructure.

Natural disasters have devastating impacts on every aspect of daily life. Some, such as the COVID-19 pandemic, occur once in a lifetime and lead to unprecedented repercussions whereas others, such as hurricanes, occur almost every year and yet still cause inevitable disruptions. Regardless of the frequency of disasters, debris management remains as one of the most critical activities to build community resilience and return a community to its pre-hurricane state (1). Storm debris is one of the main reasons for failures on infrastructure networks such as roadways, power grid, rail roads, water and natural gas pipelines, and waste management services (2). For example, roadway networks are vulnerable to post-hurricane vegetative debris in such a way that there will be failed or disrupted critical links after a hurricane because of rising water, downed trees/branches, and debris accumulation (3). If the debris is not removed from the streets, emergency responders may be delayed in carrying out their life-saving activities (4) and transportation accessibility may be difficult, or in some cases impossible, for those

victims seeking help. In addition to the roadway closures, delayed post-hurricane debris removal also has a significant impact on traffic congestion and driving behaviors of the residents (5). Reconstruction of any damaged infrastructure network can also be delayed in the long-term if debris is not cleared from the roadways (6). Moreover, hurricanes striking the Southeast U.S. in the last couple of decades highlight operational and financial disruptions caused by post-hurricane debris on transportation systems. For example, Hurricane Katrina (2005) generated 50 times more solid waste than the usual

¹Department of Civil & Environmental Engineering, FAMU & FSU College of Engineering, Tallahassee, Florida, USA

²Department of Civil Engineering, University of Twente, Enschede, The Netherlands

³Department of Computer Science and Electrical Engineering, Western Norway University of Applied Sciences, Bergen, Norway

Corresponding Author:

Alican Karaer, akaraer@fsu.edu

annual amount in Louisiana and the debris removal/disposal operations continued for more than 2 years, creating significant burden on transportation infrastructure (7). Also, during the 2004 and 2005 hurricane seasons, an average of 488 cubic yards ($\text{cy} \approx 0.76 \text{ m}^3$) vegetative debris per every mile of roadway segment was collected in Florida with a cost of \$21.5 per cy (8). More recently, Hurricane Michael (2018) caused more than 2 million cy vegetative debris in Florida Panhandle Region, and the State of Florida has spent more than \$150 million from federal emergency funds for debris removal operations (9). All in all, debris management is one of the major concerns for transportation and/or emergency agencies in the aftermath of a hurricane. Conducting a detailed debris assessment can help to improve the recovery of transportation systems through faster and cost-effective removal operations.

As a part of hurricane damage evaluation, post-hurricane debris assessment is a well-studied topic among forestry and natural hazards scholars (8, 10–15). Additionally, public agencies such as US Army Corps Engineers (16), Federal Emergency Management Agency (FEMA) (17), and Broward County, FL Emergency Management Office (18) developed post-hurricane debris volume estimation models to assist state Departments of Transportation on post-hurricane debris removal operations. These studies provided great knowledge on hurricane vegetative debris generation; however, their major concern was using field data measurements such as tree counts, diameters, and heights for the vegetation cover inputs. Also, these datasets may not be available for all trees in certain areas. Collection of such a tree database could be very expensive and time consuming, as periodic updates are required to evaluate hurricane impacts (19–21). Remote sensing, on the other hand, is a cost-effective and versatile tool that can be incorporated into hurricane debris assessment (22). Spectral indices can provide accurate estimations on land characteristics such as vegetation health (23), developed land (24), or water surfaces (25) to replace field data collection in debris assessments. Additionally, recent damage assessments studies from North Florida indicate that hurricane-induced infrastructure disruptions such as roadway closures and power outages are more likely to occur in low-income and vulnerable population areas (26–28). Thus, this study proposes a data fusion framework combining spectral and vector datasets to evaluate the vegetative debris collected in Tallahassee, FL after Hurricane Michael in 2018.

Literature Review and Research Gaps

We reviewed two main domains of research related to our study. First, traditional hurricane damage

assessment studies are summarized to identify the research gaps and potential driving factors for hurricane debris. Second, we provide a background on remote sensing-derived spectral indices to incorporate these simple, yet accurate land cover/use indicators into our framework.

Hurricane Damage and Debris Assessment

Several studies have investigated hurricane damage on infrastructure systems. For example, Hurricane Irene (2011) made \$65 million damage to the transportation network in Vermont (29) and Hurricane Andrew (1992) caused 1.4 million (44%) customers in Florida to lose power (30). Another study proposed a new index, namely Accessibility Decrease Index, to measure the delay on emergency response travel times using real-life roadway closures during Hurricane Hermine (4). Roadway disruption probabilities were also estimated using a convolutional neural network model to identify trees along the roadway from satellite images. A treefall probability estimation model was developed using precipitation, roadway density, and wind speed after Hurricanes Irene and Sandy (2012) in New Jersey (31). It was found that roadway density and wind speed were the leading factors. Another study, evaluating the power outages during five hurricanes at North and South Carolina, found that maximum wind speeds were highly correlated with power grid disruptions (32). This is completely logical, as wind speed is one of the best known hurricane impact variables (33).

In addition to the storm surge, environmental characteristics, such as soil type, land cover/use, vegetation, and elevation, were also used to predict power outages (34). Inclusion of environmental factors improved the model accuracy twice, and it was stated that environmental factors were essential in preparing the power system before a hurricane landfall. These studies expressed the significance of storm surge and environmental characteristics on evaluating the infrastructure disruptions caused by hurricanes. As expected, similar attributes for storm surge variables were observed in debris assessment studies (8, 10–15). Vegetation characteristics were identified as the most determinant factors while developing spatial predictive models on post-hurricane vegetative debris (14). Also, a survey stated that hurricane damage to and from trees was the major concern for homeowner association leaders of two different urbanizing areas, namely hurricane-prone Hillsborough and Broward Counties, Florida (15).

Apart from the storm surge-related and environmental characteristics, several studies paid attention to the impact of hurricane-related and debris-based disruptions on different socioeconomic groups while considering

vulnerability and resilience of those groups (26–28, 35–38). For example, a report from Congressional Research Services states that the African-American population with low income suffered the most from Hurricane Katrina-induced debris (36). With a focus on infrastructure disruptions, it was found that power outages after Hurricane Hermine were spatially clustered rather than being randomly distributed across the city (27). More importantly, it was found that areas with a more elderly population and low-income households were more likely to be in those clusters. More recently, a modeling framework was proposed to assist decision makers in developing resilience policy alternatives not only with respect to technical aspects, but also with respect to the socio-demographic impacts (35). The findings indicate significant differences in the power restoration times between the different age groups, ethnicity, and income levels for customers in Tallahassee, Florida, after Hurricane Hermine. Higher-income households were also found to be more resilient after Hurricane Irma in Highlands and Orange Counties, Florida (39). Note that power outages after Hurricane Hermine were mostly caused by toppled trees on the power lines. Another study analyzed power outages and roadway closures during both Hurricanes Hermine and Michael (26). The results showed that roadway closures and power outages caused by fallen trees and debris were associated with each other and vulnerable population segments (i.e., low-income populations, minority populations) from such network disruptions. These studies clearly indicate that resilience of our communities against hurricanes depends on numerous considerations including but not limited to socioeconomics, demographics, critical facility capacities, governmental and municipal capabilities, and economic status.

Debris data are more difficult to collect than infrastructure disruption data such as roadway closures and power outages. This makes it harder to evaluate the damage of a hurricane in the context of debris. This is mainly because it is difficult to quantify debris damage. US Army Corps Engineers developed the first debris estimation model using data collected from Hurricanes Frederic (1979), Hugo (1989), and Andrew (1992) (16):

$$Q = H(C)(V)(B)(S) \quad 1(16)$$

Q : Debris Volume

H : Number of Households

C : Storm category factor = {2, 8, 26, 50, 80
for Hurricane Category {1...5}}

V : Vegetation characteristics multiplier = {1.1, 1.3, 1.5}

B : Developed land multiplier = {1.0, 1.2, 1.3}

S : Precipitation multiplier = {1.0, 1.3}

Although this was an empirical model, it had the ability to estimate debris volume with a maximum of $\pm 30\%$ error. The first deterministic model was developed using the FEMA Project Worksheets, based on inputs from communities which received monetary assistance for damage after any of the seven hurricanes during the 2004 and 2005 hurricane season in Florida (12). A total of 680 Project Worksheets were collected with volume and expense information. A sample of these worksheets was matched with field-measured historical tree data (i.e., canopy cover, density), developed land cover, and wind speed. The final model developed had values of 0.77cy for low-damage storms, 4.44cy for moderate-damage storms, and 22.85cy for high-damage storms for every 100 ft. street segment (13). Following this form and using the same dataset, an average of 488cy vegetative debris with a cost of \$21.5 was calculated (8). Another study evaluated the urban forest debris after Hurricane Ike (2008) using permanent plots in Houston, TX (14). The findings of the study indicated that in situ vegetation variables explained greater variation in tree debris volume than the storm-related meteorological variables such as wind speed. In addition, Duryea et al. (10, 11) collected tree damage data from the field 2 days after Hurricane Ivan (2005) to evaluate the resilience of individual trees by their species, which is also dangerous given the hurricane aftermath conditions. Overall, these studies provided much knowledge on the generation of hurricane vegetative debris; however, the major concern was using field data measurements such as tree counts, diameters, and heights for the vegetation cover inputs. These datasets may not be available for all trees in certain areas. Collection of such a tree database could be very expensive and time consuming, as periodic updates are required to evaluate hurricane impacts. A satellite image taken before and after the hurricane can provide sufficient information about vegetation health to be used in vegetative debris assessment. Reduction on vegetation index may also provide information on tree damage which can be used to analyze the resiliency of different tree species.

Based on the extensive review of hurricane damage assessment studies, the driving factors of hurricane debris formation are identified as: (a) vegetation cover, (b) storm surge, (c) developed (built-up) land, and (d) population/socioeconomics.

Remote Sensing and Spectral Indices

Remote sensing is a cost-effective and versatile tool that can be incorporated into hurricane debris assessment (22, 40–42). Spectral indices have been developed with simple band arithmetic operations using the different reflectance patterns of specific land cover/use objects on

different spectrums of the light. Since multispectral satellite images became available with varying temporal and spatial resolutions, several spectral indices have been developed with the difference to sum ratio—so-called normalized difference—of visible spectrum, RGB (Red, Green, Blue), and invisible spectrum such as near infrared (NIR) or short-wave infra-red (SWIR). In general, the NIR and visible spectrum have been used to develop vegetation indices (VIs) whereas the SWIR has been utilized to indicate built-up (manufactured) features or water surfaces, commonly named as miscellaneous indices (MIs). Although the implementation of spectral indices varies from burned area analysis (43) to coastline change detection (44), the main focus remains on the vegetation (23, 45). An investigation on the development and applications of more than 100 VIs has been presented in a review study (46). Among these VIs, Normalized Difference Vegetation Index (NDVI) has been widely used for hurricane damage assessment purposes (20–22, 47, 48). For example, a study identified the sudden drop in NDVI values in Puerto Rico and Dominica after Hurricane Maria (21). However, it is well known that NDVI is sensitive to soil brightness and atmospheric conditions (46, 49). Although these studies present the feasibility and the accuracy of using NDVI for hurricane damage assessment purposes, to the best of the authors' knowledge, an approach to evaluate the performance of multiple spectral indices in the context of hurricane debris has not been proposed.

The current study examines five different VIs and two different MIs.

- NDVI: Normalized Difference Vegetation Index is the most commonly used vegetation index (20–22, 46–48). After launching Earth Resources Technology Satellite (ERTS)—renamed Landsat 1—in 1973, NASA funded several research projects to understand its capabilities. One of those projects, *Great Plains*, investigated the vegetative cover in the Great Plains region of central U.S. and found that the difference/sum ratio of NIR and Red reflectance values highlights healthy vegetation among other land cover/use features (50). As a normalized difference ratio, NDVI ranges from -1 to 1 . Negative values are associated with water whereas values closer to zero (-0.1 to 0.1) generally correspond to barren areas of rock, sand, or snow. Lower positive values, in the span of 0.2 to 0.4 , represent shrub and grassland whereas high positive values refer to temperate and tropical rainforest (51, 52).
- GNDVI: Green Normalized Difference Vegetation Index is similar to NDVI. However, it utilizes Green reflectance instead of Red

reflectance. The index performs better to identify the concentration of chlorophyll pigment which is essential for photosynthesis (53).

- MSAVI2: Modified Soil-Adjusted Vegetation Index (MSAVI) (49) and its revision, MSAVI2 (54), were developed to overcome the soil-brightness sensitivity of NDVI. The problem with the original Soil-Adjusted Vegetation Index (SAVI) (55) was the required input of soil-brightness correction factor (L) along with NIR and Red bands. MSAVI utilized the slope of visible density change on the feature space plot of Red and NIR brightness values to calculate the L value. Then, MSAVI2 simplified the equation using only Red and NIR bands while preserving the insensitivity on soil brightness. MSAVI2 is used in many remote-sensing applications to associate with the in situ vegetation cover (56), monitor desertification with Leaf Area Index (LAI) in China (57), or to estimate biomass (58). One major drawback of the MSAVI2 is that some overall sensitivity to detect changes on vegetation cover/amount is lost while adjusting the band arithmetic for the model to be less sensitive on the soil surface brightness (46, 59).
- MTVI2: Modified Triangular Vegetation Index (MTVI) and its revision MTVI2 were used for LAI estimation (60). This index was calculated with NIR, Red, and Green bands and it is the only narrow band vegetation index used in this study. Compared with broad band VIs, narrow band VIs were found to be more sensitive to smaller changes in the vegetation health (61).
- VARI: Visible Atmospherically Resistant Index was calculated using only the visible spectrum (62). Therefore, this index is especially useful when only RGB images are available without NIR or any other band (63). As its name suggests, VARI is more resistant to atmospheric factors such as aerosol.
- NDBI: Normalized Difference Built-up Index highlights manufactured features, such as buildings and roadways, by using the reflectance difference on SWIR and NIR. It is generally used for urban area mapping and land-use planning (24).
- MNDWI: Modified Normalized Difference Water Index highlights water land cover while suppressing the noise from vegetation, built-up land, and soil (64, 65).

Research Questions

Based on the literature reviewed, the following research questions are identified:

(RQ1) Given that land characteristics (vegetation and built development) are the most significant variables to estimate debris volume before a hurricane’s landfall (14), can spectral indices provide this information at the U.S. Census Block Group (BG) level? If so, which VI is the best for this purpose?

(RQ2) Given that individual tree damage was collected in the field shortly after hurricane to determine the resiliency of tree species (10, 11) and it is generally hard to obtain hurricane-related debris data, can reduction in VI after storm (VIΔ) provide this information to relevant agencies? If so, which VI is the best for this purpose?

(RQ3) Given that power outages and roadway closures from Hurricanes Hermine and Michael affected regions differently based on the socioeconomic differences in factors such as age, income, and the ethnicity (26–28, 35–38), is there any socioeconomic indicator related to post-hurricane vegetation debris? Can this information identify higher-risk regions in terms of debris and help debris removal operations for certain BGs?

collection of this data can be costly and time consuming with required periodic updates. With the availability and convenience of remote sensing, powered with the simple yet accurate estimations on the vigor of vegetation or density of the manufactured features, spectral indices can change the way that transportation and emergency professionals prepare for and perform vegetative debris removal operations.

Previous studies have proven the nonhomogeneous distribution of hurricane impacts on different socioeconomic groups, including those that are at-risk. Therefore, there is also a need to study the impact of socioeconomic factors on post-hurricane vegetative debris. Thus, this study promotes a data fusion framework combining multispectral satellite imagery and various vector data to evaluate post-hurricane vegetative debris. The proposed framework is illustrated in Figure 1 and the major contributions of this study are as follows:

- In terms of **practical applications**, the findings of this study can assist transportation and emergency professionals in the identification of equipment and machinery staging sites, location of temporary debris collection centers, early in-advance and more appropriate procurement of contractors, recruitment of extra staff and labor resources, and better forecasting of costs affiliated with clean-up and disposal of hurricane debris (14, 66).
- For the **debris-focused research domain**, the proposed framework demonstrates the successful integration of satellite-derived land cover/use information into small geographical units to evaluate post-hurricane debris. The proposed framework can be used to develop robust debris volume

Research Framework and Expected Contributions

Vegetative debris is one of the major concerns for recovery of the transportation network in the aftermath of a hurricane. The best strategy for timely debris removal is to identify those factors that affect debris generation. Existing studies on post-hurricane debris assessments used field-measured vegetative data such as tree height, dimension, and counts (8, 12, 14, 18). However, such a tree database may not be available for every location, and it may not include all the tree types. In addition,

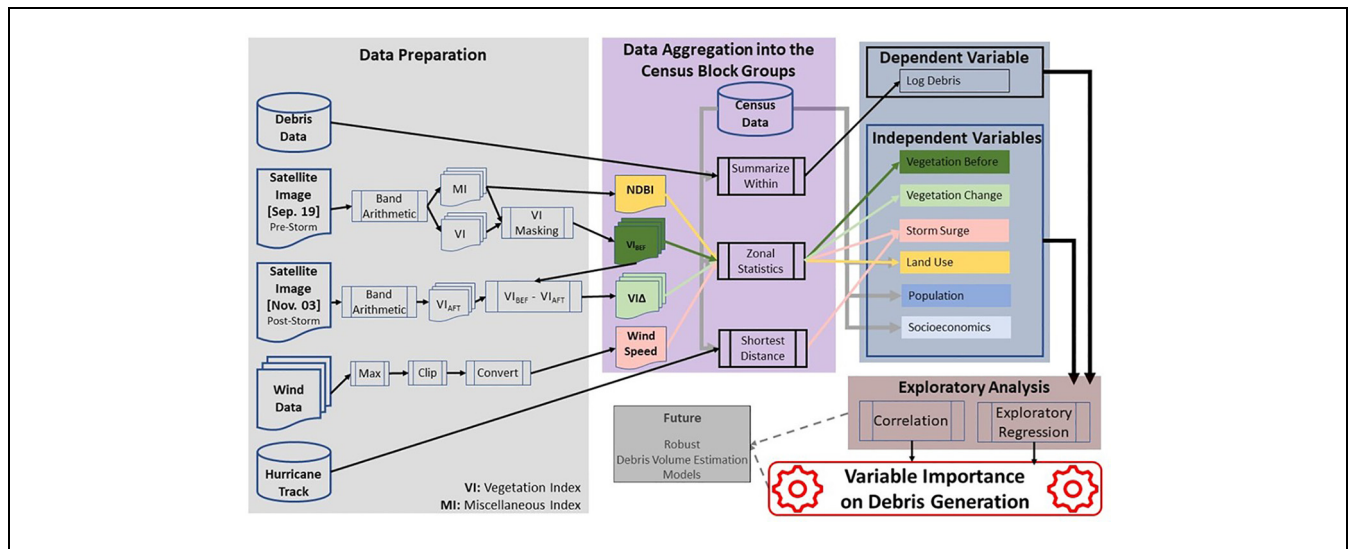


Figure 1. Proposed research framework.

prediction models at the BG level given the debris data availability.

- With a focus on **remote sensing literature**, this study evaluates the performance of five different VIs to find the most suitable one for post-hurricane debris assessment purposes. Findings have high potential for (a) replacing field measurements of pre-storm vegetation, and (b) identifying the post-storm damage on vegetation by calculating the VI reduction after storm.

Note that the objective of this study is to provide an assessment on the post-hurricane vegetative debris volume collected after Hurricane Michael in Tallahassee, FL rather than attempting to develop predictive models for the post-hurricane debris volume. Findings of this study can help develop robust prediction models with more data from multiple hurricanes and multiple communities.

Case Study Area and Data Collection

Study Area and Hurricane Michael

The study presents a U.S. Census BG-level analysis in the City of Tallahassee, Florida. A medium-size city and the state capital, Tallahassee has a population of 193,551 (as of 2018 (67)). It is also the home for two major universities, namely Florida State University and Florida Agricultural and Mechanical University. As a result, students comprise approximately 40% of the entire population (68). Additionally, more than 30 state government agency headquarters including the Capitol Building, Florida Supreme Court, and Florida Governor's Mansion are in Tallahassee.

The urban forests in Tallahassee consist of short-lived, weak-wooded species such as Carolina laurelcherry, water oak, laurel oak, and camphor tree. These species alone compromise 37% of the urban forest (69). More importantly, tree canopy covers 55% of the total land, and canopy roads are part of the southern culture (70). Therefore, post-hurricane vegetative debris removal is an essential task for a fast recovery of the entire transportation infrastructure network.

Figure 2 depicts the study area along with its relative location to the path of Hurricane Michael and population density of the BGs. Geocoded city limits were extracted from the Tallahassee–Leon County GeoData Hub (71) and those BGs completely within this limits were analyzed. As the university campuses are in the central west side of the town, the BGs in this area present higher population densities.

Note that Hurricane Michael's path in Figure 2 is categorized according to the Saffir–Simpson Hurricane Wind Scale (72, 73). This scale indicates that Tropical

Storm refers to 39 to 73 mph wind speed, Category 1 refers to 74 to 95 mph wind speed, Category 2 refers to 96 to 110 mph, Category 3 refers to 111 to 129 mph, Category 4 refers to 130 to 156 mph and Category 5 refers to 157 mph or higher wind speeds. More details on the wind speeds for the study area are presented in the data description section along with other data sources.

A report from National Oceanic and Atmospheric Administration (NOAA) states that the Southeast region of the U.S. had suffered 15 named storms, eight hurricanes, and two major hurricanes in 2018, which is considerably higher than the 1981 to 2010 average of 12.1 named storms, 6.4 hurricanes, and 2.7 major hurricanes (74). Among these severe weather events, Hurricane Michael was a highly destructive hurricane which crushed the entire Florida Panhandle in 2018. It was the first Category 5 hurricane to strike the mainland U.S. since Hurricane Andrew in 1992 (75). Michael made a landfall with peak winds of 160 mph (260 km/h) and affected the states of Florida, Georgia, Alabama, both Carolinas, and even Virginia, causing directly or indirectly the deaths of 74 people (75). The cost of the total damage caused by Hurricane Michael was estimated to be more than \$25 billion by NOAA's National Centers for Environmental Information (74).

Data Collection and Preparation

In this paper, the vector data such as debris collection records and those that are related to the socioeconomics as well as the raster (imagery) data such as satellite images and wind gusts were collected from various sources. ArcGIS Pro v2.5 was employed to process all these datasets. The timeline for Hurricane Michael and the data collection process is presented in Figure 3. The collected data are introduced separately along with their pre-processing steps. Note that S2A and S2B stand for the satellites Sentinel-2A and Sentinel-2B, respectively. These are identical satellites orbiting across opposite sides of the world. Additionally, L1C refers to the top level of pre-processing for the images acquired from Sentinel-2 satellites. Basically, L1C products provide the top-of-atmosphere reflectance in fixed cartographic geometry.

Debris Data. The City of Tallahassee provided the debris data used in this paper. Some 9,716 debris collection points were recorded with the information on volume and coordinates for loading and unloading locations. The data have been cleaned by removing entries of zero volumes and those that had the same locations for loading and unloading. Presumably, some of the collecting points were missing the loading location coordinates and they were populated with the unloading location

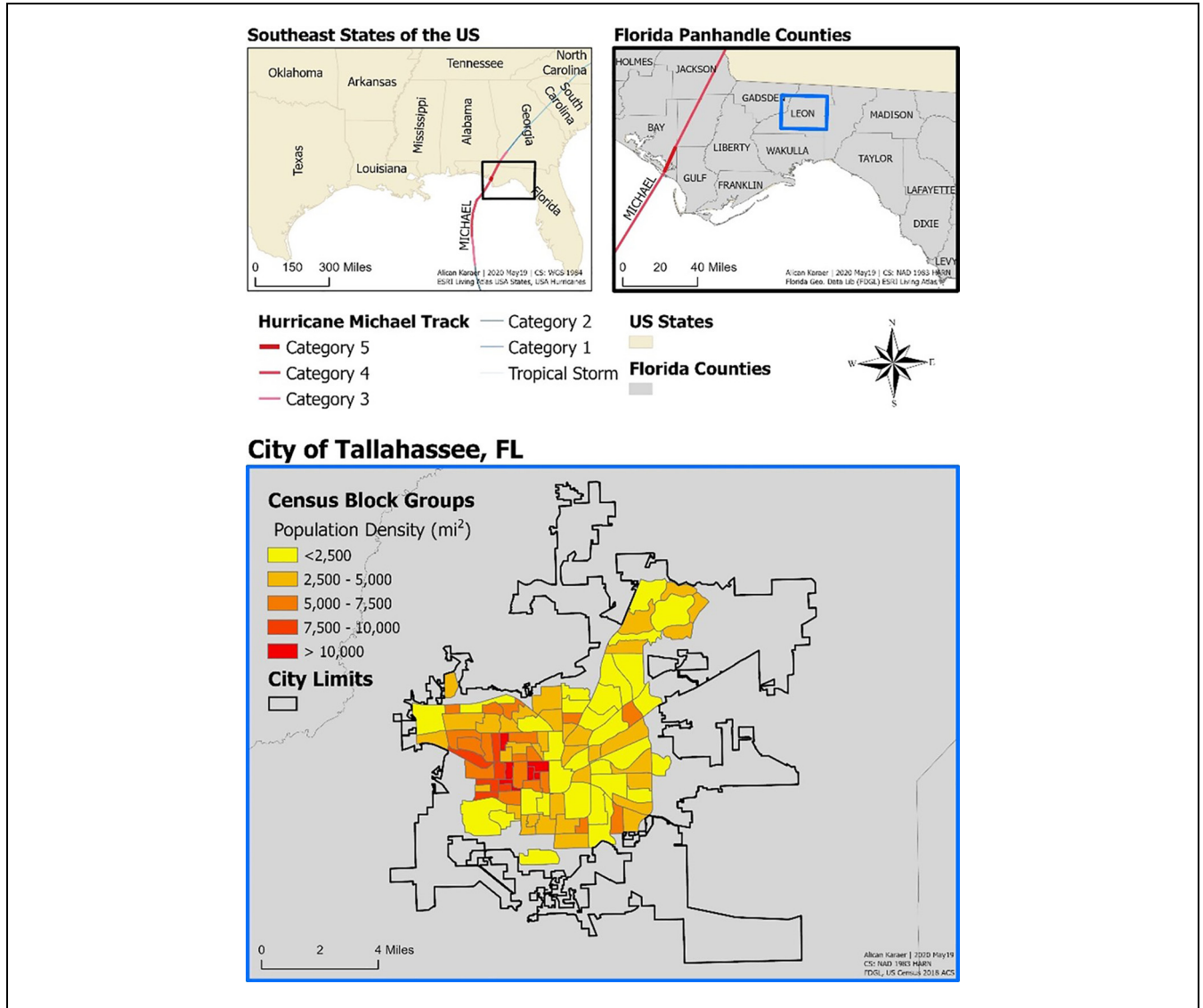


Figure 2. The study area with population density and its relative location to the track of Hurricane Michael.

coordinates. This could have resulted in a biased aggregation of the debris volumes into the 95 BGs. After the data cleaning, the remaining 7,820 debris collection points were aggregated into the BGs based on where the debris was collected from. Figure 4 indicates the debris collection points and their aggregation into BGs with their numerical and spatial distributions. Note that “n” represents the total number of debris collection points in the upper distribution graph whereas “n” represents the number of BGs in the lower distribution graphs. Additionally, the count on y-axis indicates the partial number of “n” in each graph.

As the total debris volume in BGs seems to follow an exponential distribution, natural log of the total debris volume is calculated and used as the dependent variable for the exploratory analysis. Note that the debris

collection points are the locations where a stack or a pile of vegetative debris was removed by the city. These stacks may consist of a single fallen tree or multiple branches and trunks from the surrounding of the collection point. However, the debris volume was aggregated into BGs as the target geographical unit. This is a critical assumption made in this paper.

Population Data. Population data were extracted from the U.S. Census Bureau 2018 American Community Survey (ACS) (76) using the Florida Geographic Data Library (FGDL), a mechanism for distributing spatial data throughout the State of Florida (77). Note that ACS is conducted by the U.S. Census Bureau every year by sampling the entire population. Unlike the every-10-year

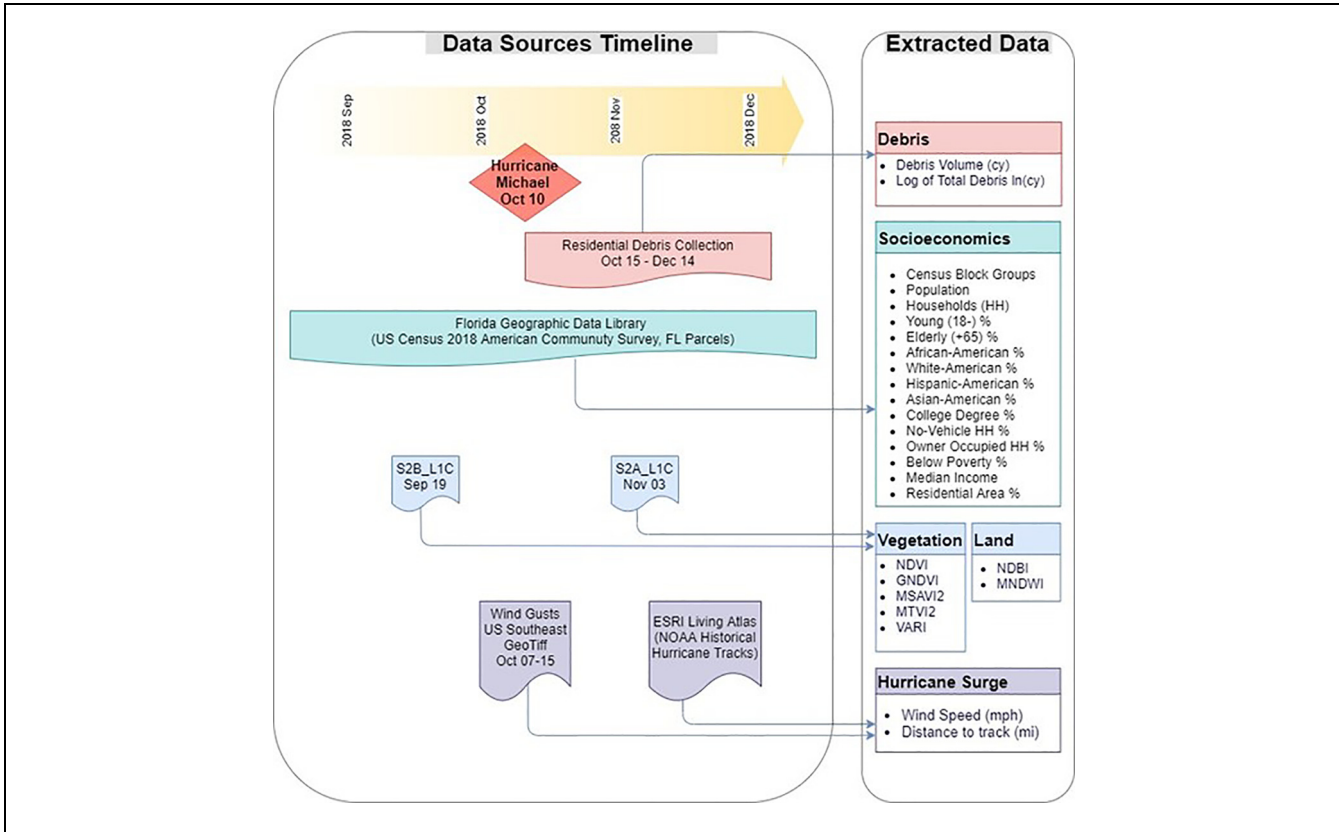


Figure 3. Data sources and acquisition timeline.

census, ACS is based on estimates and utilized by federal and state governments. ACS reveals socioeconomic characteristics (i.e., race, education, age, and income) of the population in geographic units from states to census blocks (76).

Remote Sensing Data. The Copernicus Project of European Space Agency provides various free earth observatory data, which have been used for various purposes such as flood detection (78) or air quality monitoring (79). In this study, georectified Sentinel-2 satellite imagery, obtained from the Copernicus Open Access Hub (80), was used to calculate the land cover/use spectral indices. As Table 1 indicates, Sentinel-2 provides 12 bands for different spectrums of the light with varying spectral resolutions for each band within (10–60 m (~32 ft.–197 ft.)/pixel) spatial resolution. This study used only the NIR (Band 8) and the SWIR (Band 11) with the visible spectrum in Bands 2, 3, 4 for “Blue”, “Green”, and “Red,” respectively.

Before and after images were selected considering the cloud coverage over the study area. Given that Hurricane Michael was active between October 07 and 15 in 2018 (75), the acquisition date for the before image was September 19, and it was November 3 for the after image.

After downloading the images and mapping them with aforementioned composite bands, images were clipped based on the Tallahassee City limits extracted from the Tallahassee–Leon County GIS GeoData Hub (71). Figure 5 indicates full size and clipped images in true color format. To enhance the images with sharp contrast, the display was set to 0.25 percent-clip rendering. Also, as the magnified small images from Tallahassee clips indicate, 10 m/pixel resolution provides sufficient details to generalize the vegetative cover at the BG level.

After obtaining the before and after Hurricane Michael images with a clean view over the study area, different indices were calculated for the vegetation, water, and manufactured features. Table 2 shows these indices along with their interest land cover/use, mathematical definition, and the reference study. Spectral VIs are the simplest measures of general quantity or vigor of green vegetation. VIs are generally inspired by the fact that plants absorb visible light for photosynthesis and reflect back most of the NIR spectrum simply because the longer wavelengths do not provide sufficient energy for photosynthesis. On the other hand, MIs highlight land cover features other than the vegetation. Such indices utilize the reflectance difference on the visible spectrum and SWIR.

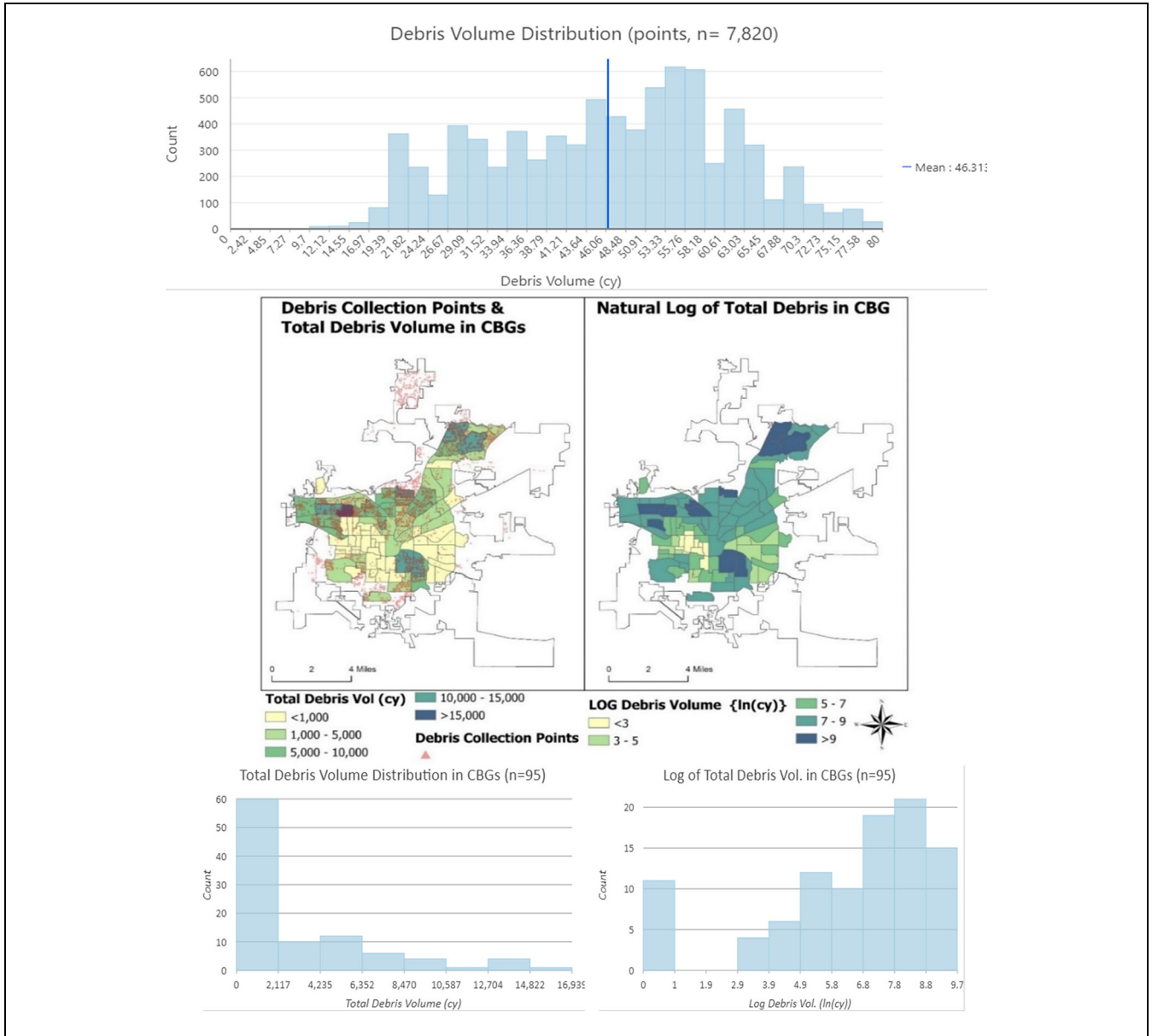


Figure 4. Debris data points and aggregated debris volume into the BGs. The y-axes of the distributions represent the number of “n” in each graph.

To eliminate the noise on VIs from the built-up areas and water surfaces, areas with the high values of NDBI and MNDWI were masked out. The masking process is summarized in Figure 6. After masking the vegetation indices, vegetation change ($VI\Delta$) was calculated using the vegetation change of the before image (VI_{BEF}) and after image (VI_{AFT}) as follows:

$$VI\Delta = VI_{BEF} - VI_{AFT} \quad 2$$

To statistically analyze the significance of VI_{BEF} and $VI\Delta$ on the debris amount prediction, the average values were calculated for each of the BGs using the zonal statistics

toolbox. This tool considers each BG as a zone and calculates the mean of pixel values in each zone.

Wind Speed. Hurricane surge characteristics, such as wind speed, are known to have a significant impact on vegetation loss and debris generation (14, 16–18) where the higher wind speeds cause more damage. In this regard, the maximum wind gusts (average wind speeds within ~20 s.) data were provided by StormGeo Inc. for every 3 h period between October 7 and October 15. A total of 72 georectified images were obtained.

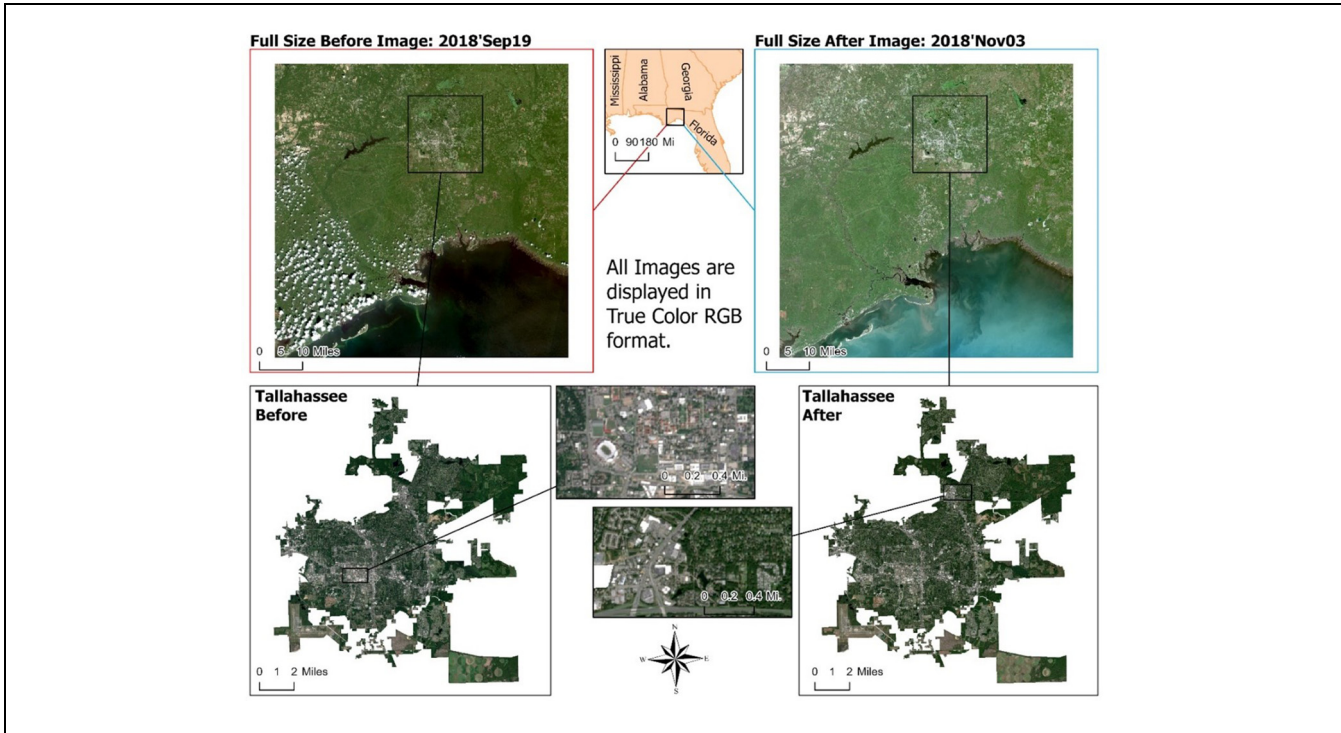


Figure 5. Before and after Sentinel-2 images and extracted clips for Tallahassee. MNDWI = Modified Normalized Difference Water Index; NDBI = Normalized Difference Built-up Index; VI = Vegetation Index.

Table 1. Sentinel-2 Bands and their Spatial Resolution. Adopted from Wikipedia (81)

Sentinel-2 bands	Central wavelength (μm)	Resolution (m)
Band 1 – Coastal Aerosol	0.443	60
Band 2 – Blue	0.490	10
Band 3 – Green	0.560	10
Band 4 – Red	0.665	10
Band 5 – Vegetation Red Edge	0.705	20
Band 6 – Vegetation Red Edge	0.740	20
Band 7 – Vegetation Red Edge	0.783	20
Band 8 – NIR	0.842	10
Band 8A – Vegetation Red Edge	0.865	20
Band 9 – Water Vapor	0.945	60
Band 10 – SWIR - Cirrus	1.375	60
Band 11 – SWIR	1.610	20
Band 12 – SWIR	2.190	20

Note: NIR = near infra-red; SWIR = short-wave infra-red.

Figure 7 depicts the process of extracting wind speeds for each BG. First, maximum values for each pixel were extracted from those 72 images as shown in Figure 7a. After the nearest neighborhood resampling and unit conversion from meter per second to mile per hour (Figure 7b), wind speeds for the study area were extracted using the Tallahassee City limits similar to the process for

Sentinel-2 images (Figure 7c). Finally, the average wind speeds were calculated within each BG using the zonal statistics toolbox. Note that the scales between Figure 7(a, b) and Figure 7c are different, and based on the data provided by StormGeo Inc., the wind speeds ranged between 70 mph and 79 mph in the study area, which corresponds to a Tropical Storm and Category 1 hurricane in the Saffir–Simpson Hurricane Wind Scale, respectively.

Finally, the descriptive statistics of the final dataset are provided in Table 3. The descriptive statistics are important to understand the potential of using VIΔ as the debris damage variable regarding the RQ2. The discussion is provided in the results and discussion section.

Methodology

In this paper, the main goal is to assess the post-hurricane vegetative debris in Tallahassee, FL after Hurricane Michael using an exploratory data analysis. Two-way correlation analysis was used to oversee the relationships among all datasets, and significance of correlation was calculated between each independent variable and the dependent debris variable. Second, a variable importance metric was developed by evaluating all possible combinations of independent variables in hypothetical regression models.

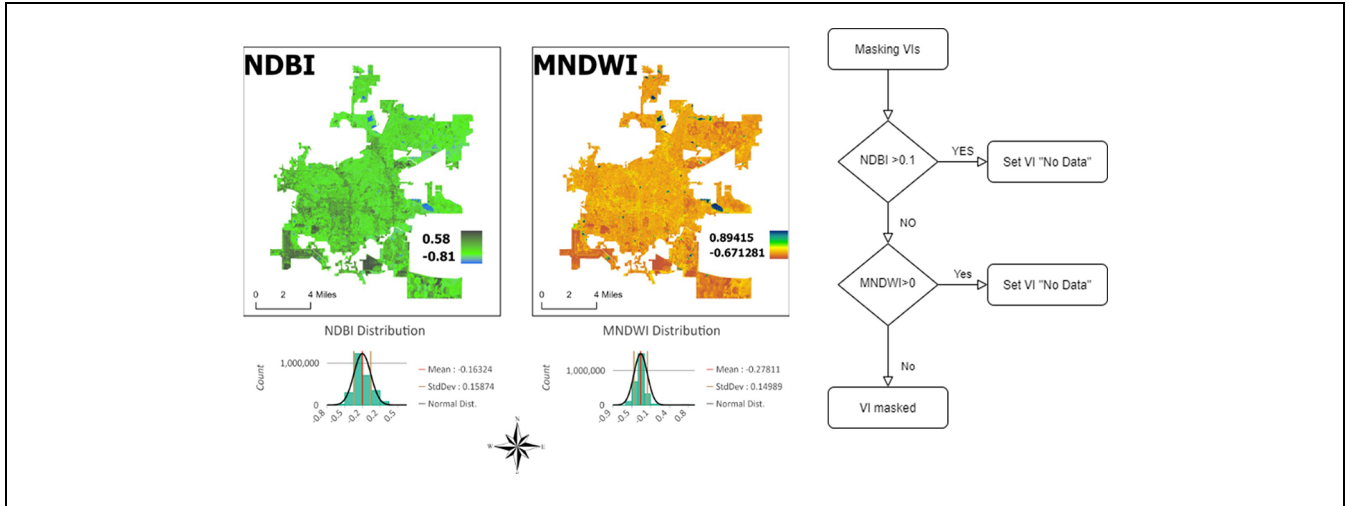


Figure 6. VI masking process.
MNDWI = Modified Normalized Difference Water Index; NDBI = Normalized Difference Built-up Index; VI = Vegetation Index.

Table 2. Derived Spectral Indices

Index	Interest land cover	Definition	Reference
NDVI	Vegetation	$\frac{(NIR - Red)}{(NIR + Red)}$	Rouse et al. (50)
GNDVI	Vegetation	$\frac{(NIR - Green)}{(NIR + Green)}$	Buschmann and Nagel (53)
MSAVI2	Vegetation	$2 * NIR + 1 - \sqrt{(2 * NIR + 1)^2 - 8(NIR - Red)}$	Qi et al. (54)
MTVI2	Vegetation	$\frac{1.5[1.2(NIR - Green)^2 - 2.5(Red - Green)]}{\sqrt{(2 * NIR + 1)^2 - (6 * NIR - 5 * \sqrt{Red})} - 0.5}$	Haboudane et al. (60)
VARI	Vegetation	$\frac{(Green - Red)}{(Green + Red - Blue)}$	Gitelson et al. (62)
NDBI	Urban	$\frac{(SWIR - NIR)}{(SWIR + NIR)}$	Zha et al. (24)
MNDWI	Water	$\frac{(Green - SWIR)}{(Green + SWIR)}$	Xu (64)

Note: GNDVI = Green Normalized Difference Vegetation Index; MNDWI = Modified Normalized Difference Water Index; NDBI = Normalized Difference Built-up Index; NDVI = Normalized Difference Vegetation Index; MSAVI2 = Modified Soil-Adjusted Vegetation Index (revised); MTVI2 = Modified Triangular Vegetation Index (revised); VARI = Visible Atmospherically Resistant Index

Correlation

Pearson Correlation Coefficient (r) is a well-known measure of similarity measure of two variables (82). It is calculated with element-wise multiplication of those variables after normalization to standard normal distribution. This type of normalization of correlation is a common approach to test the similarities of variables with different units (i.e., debris volume [cy] and wind speed [mph]). Mathematically, Pearson’s r can be defined as:

$$r = \frac{E[(X - \mu_X)(Y - \mu_Y)]}{\sigma_X \sigma_Y} \quad 3$$

where *r* defines the correlation between *X* and *Y* and takes a place in [-1,1]. -1 indicates a perfect inverse correlation, and 1 indicating a perfect correlation between the tested variables. Please note that the *r* defines the strength and direction of the linear relationship between *X* and *Y*. However, the reliability of this metric also depends on the sample size. Therefore, the significance of correlation coefficients with hurricane debris was calculated using two-tailed *t*-test:

$$t_{score} = \frac{r\sqrt{n-2}}{\sqrt{1-r^2}} \quad 4$$

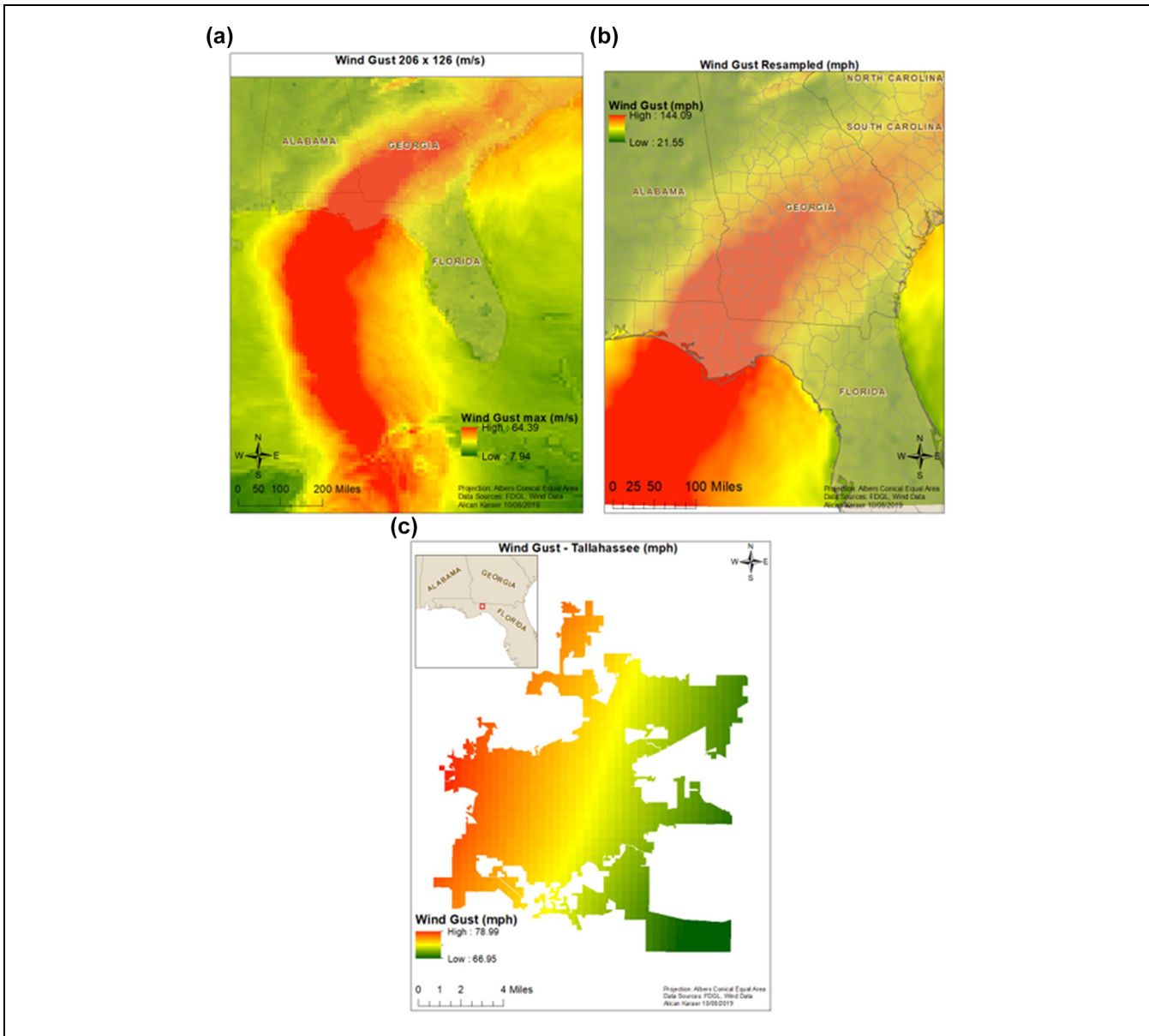


Figure 7. Wind data extraction for BGs. (a) Maximum wind gusts (m/s) between October 7 and 15, (b) resampled and converted wind gusts (mph), and (c) extraction of the study area.

where n represent the number of counties (95) as the sample size and r is again the correlation coefficient. Based on this test, the correlation between each independent variable and debris volume were identified at 90%, 95%, and 99% significance level.

Exploratory Regression

Exploratory regression is a tool provided in the GIS software used in this study. This tool can evaluate all possible combinations of the explanatory variables, searching for regression models that can best explain the dependent variable with regards to the user-specified criteria (83).

As aforementioned, the aim of this study is to identify variable importance rather than developing predictive models. Indeed, the debris data used in this study were collected for a relatively small section of the full hurricane impact area and from only a single hurricane. This would not be enough to represent the complex nature of hurricane-caused debris. However, this tool provides statistics about the variable coefficients which can be used solely for the purposes of exploratory data analysis to evaluate the importance of predefined independent variables on explaining the variance of the debris dataset.

The importance statistics refer to the significance and persistence of each independent variable by calculating

Table 3. Final Data Descriptive Statistics

Variables	Count	Min	Max	Mean	SD	Definition
Debris Total (cy)	95	0	16,939	3,038.17	3,913.7	Total volume of collected vegetative debris in BGs
Log Debris (ln (cy))	95	0	9.74	6.46	2.64	Log total volume of collected vegetative debris in BGs
NDVI _{BEF}	95	0.28	0.62	0.52	0.07	Average NDVI before Michael in BGs
GNDVI _{BEF}	95	0.26	0.48	0.41	0.05	Average GNDVI before Michael in BGs
MSAVI2 _{BEF}	95	0.41	0.76	0.66	0.07	Average MSAVI2 before Michael in BGs
MTVI2 _{BEF}	95	0.33	0.49	0.42	0.04	Average MTVI2 before Michael in BGs
VARI _{BEF}	95	0.11	0.86	0.55	0.16	Average VARI before Michael in BGs
NDVIΔ	95	-0.02	0.02	0.00	0.01	Average NDVI reduction after Michael in BGs
GNDVIΔ	95	-0.03	0.00	-0.01	0.01	Average GNDVI reduction after Michael in BGs
MSAVI2Δ	95	-0.02	0.02	0.00	0.01	Average MSAVI2 reduction after Michael in BGs
MTVI2Δ	95	-0.03	-0.01	-0.02	0.01	Average MTVI2 reduction after Michael in BGs
VARIΔ	95	-0.20	0.07	-0.02	0.04	Average VARI reduction after Michael in BGs
Wind Spd (mph)	95	72.62	78.23	75.09	1.39	Average wind gust (speed) in BGs
ShortDist (mi)	95	46.48	54.60	51.10	1.82	Shortest distance from BG to Hurricane Track
NDBI	95	-0.29	0.01	-0.15	0.06	Average NDBI before Michael in BGs
Residential Area %	95	0.00	83.35	45.90	21.65	Percentage area of residential parcel in BG
Area (mi ²)	95	0.06	1.49	0.44	0.28	Area of BG
PopD. (mi ⁻²)	95	656.46	22,266.67	4,465.12	3,386.50	Population per sq. mile in BGs
Total Pop.	95	480	3,095	1,513.5	653.18	Total population in BG
Households	95	0.00	1,652.00	590.18	327.53	Number of households in BG
Young (18-) (%)	95	0.00	38.47	14.46	9.55	Percentage of 18 years and younger population in BGs
Elderly (65 +) (%)	95	0.00	49.23	11.49	10.46	Percentage of 65 years and older population in BGs
African-American (%)	95	0.00	98.70	35.06	26.01	Percentage of African-American population in BGs
White-American (%)	95	1.30	98.10	52.35	24.93	Percentage of White-American population in BGs
Hispanic-American (%)	95	0.00	36.08	6.92	6.13	Percentage of Hispanic-American population in BGs
Asian-American (%)	95	0.00	28.40	3.19	4.70	Percentage of Asian-American population in BGs
College Degree (%)	95	0.00	60.27	24.11	16.70	Percentage of people graduated from a college in BGs
Median Income (\$)	95	0.00	129,667	42,905	27,470	Median income of households in BGs
Owner Occ. HH (%)	95	0.00	100.00	35.64	29.52	Percentage of owner-occupied households in BGs
No-Vehicle HH (%)	95	0.00	21.44	4.10	4.32	Percentage of households with no vehicle in BGs
Below Poverty (%)	95	0.00	73.18	26.54	21.79	Percentage of people below poverty level in BGs

Note: BG = US Census Block Group; PopD. = Population Density; Total Pop. = Total Population; HH = Household.

□ Debris Volume ■ Vegetation Before ■ Storm Surge ■ Land Use ■ Population ■ Vegetation Change ■ Socioeconomics.

the number of models in which the variable’s coefficient was statistically significant (p -value < 0.1) and the percentages of those significant coefficients with negative and positive values. For example, an independent variable with a high percentage of significance and a high percentage of positive coefficients indicates that the variable has a persistent positive correlation with the dependent variable. Using these statistics, a variable importance metric is developed:

$$VariableImportance(\%) = Significance\% * \max(Negative\%, Positive\%) * 100 \quad 5$$

Note that p -value < 0.1 for coefficients suggests that the independent variables were evaluated at 90% significance level. This is the only user-defined criterion on using the exploratory regression tool in this study which is logically adopted in most regression models.

Results and Discussions

This study presents an exploratory data analysis to determine the factors creating hurricane debris with a specific focus on enhancing the resilience of infrastructure systems through better planned and performed debris removal. A data fusion-based framework was proposed

to combine spectral and vector datasets in such a way that vegetative debris collected after Hurricane Michael in Tallahassee, Florida can be evaluated with four major groups of datasets.

The first and most important group of data represents the vegetation characteristics of each BG with five commonly known VIs. They were tested to better explain the variance on the debris volume in terms of pre-storm conditions (VI_{BEF}) and reduction after the storm (VIA). This is one of the most important contributions of this study as, to the best of our knowledge, this is the first study to evaluate the association of multiple VIs with actual hurricane debris data. The second group of data represents the storm surge, wind speed, and shortest distance to the hurricane’s path. Although Hurricane Michael did not pass through the City of Tallahassee directly, these variables still represent the impact of the hurricane on the city. The third dataset represents the land-use characteristics. In addition to an MI, classified parcels were tested to best explain the post-hurricane vegetative debris. Total area of each BG was also included, as the dependent variable represents the debris volume collected within each of the BGs. Finally, the fourth dataset represents the socioeconomics of each BG, including age, race, education, and income distribution of the households. Inclusion of this dataset was inspired by the previous hurricane damage assessment studies conducted in the same study area. For example, it was found out that geographical units with a more elderly population and low-income households were likely to be located in areas with a high risk of roadway closures and power outages after Hurricane Hermine and Michael (26, 27).

Observations from the descriptive analysis (Table 3) indicate that the VIA values were significantly small compared with the previous study findings (21, 48). Average reductions on $MSAVI2\Delta$ and $NDVI\Delta$ were found to be less than 0.005, while the other VIA s showed an increase with the negative change values. On the other hand, average reductions of 0.2 and 0.35 were observed on $NDVIs$ after Hurricane Maria in Puerto Rico and Dominica (21) and in the coastal Alabama after Hurricane Katrina (48), respectively. This can be attributed to the 45-day gap between before and after images used in this study, as the $NDVIs$ returned to normal values after 1.5 months in Puerto Rico and Dominica (21). However, the reduction in $NDVI$ still remained in coastal Alabama even after a year (48). This is highly related with the land cover and urbanization level of the studied areas, as well as the direct impact of the hurricane surge. As such, estuarine emergent wetland vegetation with increased salinity in coastal Alabama was found to be the most sensitive habitat with the least improvement on $NDVI$ values even after a year. Additionally, for both Puerto Rico and Dominica, the cloud forest was found the most sensitive

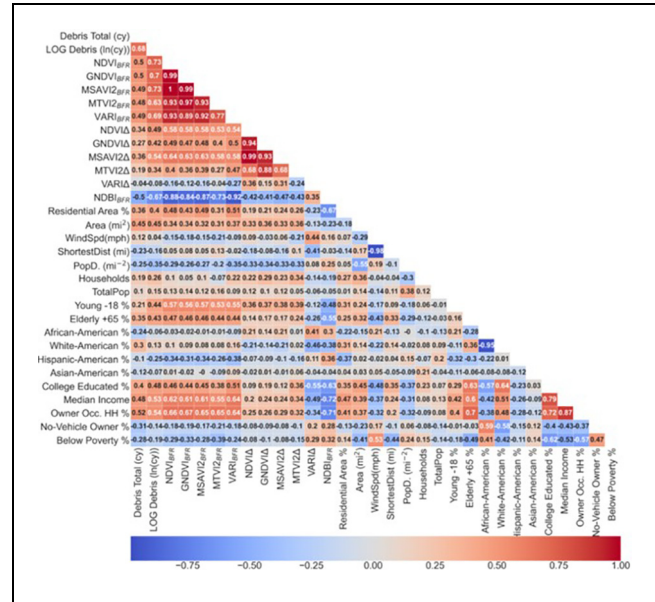


Figure 8. Two-way correlation analysis. BG = US Census Block Group; PopD. = Population Density; Total Pop. = Total Population; HH = Household.

habitat, but it recovered quickly compared with the wetlands. Also, both studies examined the landfall regions where the maximum hurricane surges were observed. Therefore, it makes sense that we observe lower VIA s in our study area. On the other hand, an average of VI decrease at the BG level may not be able to indicate the direct relationships especially in a region reasonably away from the hurricane impact area. Therefore, there is a need to investigate the exploratory results further to accurately answer the RQ2.

Results from the two-way correlation analysis are illustrated in Figure 8, indicating the correlation across all datasets. Note that the red shade indicates a strong positive correlation, closer to the correlation coefficient, $r = 1$, whereas the blue shade indicates a strong inverse correlation closer to $r = -1$. VI_{BEF} variables presents the largest correlation with debris variables, and this followed by the land-use characteristics index ($NDBI$). This finding, alone, answers the RQ1: land characteristics (vegetation and built-in environment) are the most determinant variables to estimate debris volume before the landfall (14) and spectral indices can provide similar information obtained from field-measured data. Also, $MSAVI2_{BEF}$ $NDVI_{BEF}$ outperform any other independent variables with a correlation value of $r = 0.73$ to the log of debris volume. Based on the $r > 0.5$ threshold, all VI_{BEF} variables, but only $MSAVI2\Delta$ from VIA variables ($r = 0.54$) as well as $NDBI$ ($r = -0.67$) and well-being variables such as Median Income ($r = 0.53$) and Owner Occupied HH % ($r = 0.54$) are found to be correlated with the log of debris volume.

Variables	Correlation Significance Level						Exploratory Regression Results			
	Total Debris			Log of Total Debris			% Significant Coefficient (α = 0.1)	% Negative Coefficient	% Positive Coefficient	Importance Metric %
	90%	95%	99%	90%	95%	99%				
NDVI _{BEF}	✓	✓	✓	✓	✓	✓	85.74	8.37	91.63	78.56
GNDVI _{BEF}	✓	✓	✓	✓	✓	✓	90.08	23.86	76.14	68.59
MSAVI2 _{BEF}	✓	✓	✓	✓	✓	✓	85.73	0.14	99.86	85.61
MPTVI _{BEF}	✓	✓	✓	✓	✓	✓	83.95	35.49	64.51	54.16
VI _{BEF}	✓	✓	✓	✓	✓	✓	59.45	14.98	85.02	50.54
NDVI _A	✓	✓	✓	✓	✓	✓	63.29	15.55	84.45	53.45
GNDVI _A	✓	✓	✓	✓	✓	✓	47.71	25.94	74.06	35.33
MSAVI2 _A	✓	✓	✓	✓	✓	✓	73.99	0.41	99.59	73.69
MPTVI _A	✓	x	x	✓	✓	✓	26.51	39.66	60.34	16.00
VARIA	x	x	x	x	x	x	29.25	33.16	66.84	10.55
Wind Spd (mph)	x	x	x	x	x	x	86.7	14.08	85.92	74.49
ShortDist (mi)	✓	✓	✓	x	x	x	95.06	99.99	0.01	95.05
NDBI	✓	✓	✓	✓	✓	✓	63.94	94.81	5.19	60.62
Residential Area %	✓	✓	✓	✓	✓	✓	40.9	15.3	84.7	34.64
Area (mi ²)	✓	✓	✓	✓	✓	✓	98.97	0	100	98.97
PopD. (mi ⁻²)	✓	✓	✓	✓	✓	✓	66.12	99.77	0.23	65.97
Total Pop.	x	x	x	x	x	x	23.96	0.03	99.97	23.95
Household	✓	x	x	✓	✓	✓	73.36	1.1	98.9	72.55
Young (18+) (%)	✓	✓	✓	✓	✓	✓	41.42	0.09	99.91	41.38
Elderly (65+) (%)	✓	✓	✓	✓	✓	✓	59.13	0.33	99.67	58.03
African-American (%)	✓	✓	✓	x	x	x	21.06	42.26	57.74	11.16
White-American (%)	✓	✓	✓	x	x	x	25.48	35.27	64.73	16.49
Hispanic-American (%)	x	x	x	✓	✓	✓	12.2	66.53	33.47	8.12
Asian-American (%)	x	x	x	x	x	x	18.05	98.35	1.65	17.75
College Degree (%)	✓	✓	✓	✓	✓	✓	83.32	1.14	98.86	82.37
Median Income (\$)	✓	✓	✓	✓	✓	✓	64.77	4.16	95.84	62.08
Owner Occ. HH (%)	✓	✓	✓	✓	✓	✓	58.47	5.34	94.66	55.35
No. Vehicle HH (%)	✓	✓	✓	x	x	x	2.52	42.57	57.43	11.45
Below Poverty (%)	✓	✓	✓	x	x	x	18.83	39.43	60.57	11.41

Figure 9. Variable importance display. BG = US Census Block Group; PopD. = Population Density; Total Pop. = Total Population; HH = Household.

It is worth mentioning that vegetation cover does not present an equal distribution among all the BGs according to the correlation matrix, and there is a big environmental injustice issue especially based on the income levels. The lower left side of the matrix (Figure 8) highlights this issue where income variables intersect with VI_{BEF} variables. It can be observed that the dark red colors associated with the high-income variables turn to dark blue colors for the poverty variables. Unfortunately, we also see a similar pattern when we focus on racial differences. It can be observed that BGs with higher White-American population have higher rates of vegetation land cover. There could be several reasons for these differences; however, the proposed framework integrates the remote sensing-derived environmental characteristics into the census data, and can be used to further analyze socio-ecological dynamics or urban sustainability (84).

The significance of correlation coefficients between debris variables and all other independent variables and the variable importance results of the exploratory regression tool are presented in Figure 9. Also, the developed importance metric quantifies and visualizes the impact of each independent variable on the hurricane-caused generation of vegetative debris. Results indicate that MSAVI2Δ has a high potential to represent the post-hurricane debris damage at the BG level while answering the RQ2. In addition, it was observed that causality of storm surge variables is increased when we consider the direction (i.e., negative or positive) of the coefficient. However, the most interesting results are observed on the well-being variables. According to these results, larger volume of debris was observed at the higher income

BGs. This is the opposite result based on the relationship between income levels and hurricane damage observed through the power outages after Hurricane Hermine (27). This could be attributed to the Tallahassee residents with higher income preferring to live in less urbanized areas covered with numerous trees contributing to more debris. This can also be observed from the correlation matrix (Figure 8) between the well-being variables and VI_{BEF} variables. Despite the larger impact of debris, the infrastructure in high-income areas could be better maintained or renewed so that the power outages can be solved faster compared with low-income communities. However, the findings support that the areas with more elderly people are more likely to suffer from hurricane vegetative debris. With that partially being the answer of RQ3, there is a need to analyze a larger region with more diverse socioeconomics and hurricane impact so as to determine the impact of hurricane debris on different socioeconomic groups more clearly.

Conclusions

There will be failed or disrupted segments on a transportation network after a hurricane as a function of rising water, downed trees/branches, and debris accumulation (3). Therefore, post-hurricane vegetative debris is one of the key concerns for the transportation network recovery in the aftermath of a hurricane. The best strategy for timely debris removal is to identify factors of debris generation. Therefore, this study promotes a data fusion framework by combining spectral and vector datasets in such a way that vegetative debris collected after Hurricane Michael in Tallahassee, Florida can be evaluated with four major groups of datasets. The first group represents the vegetation in each BG comparing five different spectral VIs derived from Sentinel-2 imagery for the pre-storm conditions (VI_{BEF}) and post-storm reduction (VIΔ), and the second group is related to the storm surge with predictable variables even before the hurricane hits (i.e., wind speed or distance to the track). The third group depicts the land-use characteristics with another spectral index highlighting the density of built-up area in BGs, and the fourth group of data represents the socioeconomics of each BG, including age, race, education, and income distribution of the households. Inclusion of this dataset was inspired by the previous hurricane damage assessment studies conducted in the same study area. For example, it was found out that geographical units with a more elderly population and low-income households were likely to be located in areas with a high risk of roadway closures and power outages after Hurricane Hermine and Michael (26–28).

Data integration and correlation analysis indicates that MSAVI2 is slightly better than NDVI in representing the variation in hurricane-caused vegetative debris,

and both can be used instead of field data collection. This is one of the most important contributions of this paper, as previous debris assessment studies used tree damage data collected from the field. In addition to the vegetation, NDBI can also represent the land-use characteristics with a higher correlation than the storm surge variables.

Regarding the socioeconomic variables, larger volume of debris was observed at the higher-income BGs. This is the opposite result based on the relationship between income levels and hurricane damage observed through the power outages after Hurricane Hermine (27). This could be attributed to the Tallahassee residents with higher income preferring to live in less urbanized areas covered with numerous trees, contributing to more debris. This can also be observed from the correlation between well-being variables and VI_{BEF} variables. Despite the impact of debris being higher, the infrastructure in high-income areas may be better maintained or renewed so that power outages can be solved more quickly compared with low-income communities. However, the findings support that the areas with more elderly people are more likely to suffer from hurricane vegetative debris.

Findings of this study can assist transportation and emergency professionals in the identification of equipment and machinery staging sites, location of temporary debris collection centers, early in-advance and more appropriate procurement of contractors, recruitment of extra staff and labor resources, and better forecasting of costs affiliated with clean-up and disposal of hurricane debris.

Despite the innovative approach and promising results, we faced some practical challenges in this study that we will address in the next steps of our research. First, the study area is relatively small compared with the hurricane impact area, and this leads to a limited variation on the wind speeds (i.e., 70–79 mph wind speeds). Analysis of the impacts of such a massive disaster on diverse communities by focusing only on 95 census BGs (because of debris collection data availability) may also be affected by some spatial bias. Second, the best images (cloud-free) were obtained with a 46-day gap in between before and after images. Considering the fall season foliage change, this gap could have a significant impact on the vegetation change analysis. Nevertheless, no positive change (reduction) in vegetation was observed in any VI. This could be attributed to two reasons: (a) recovery operations (i.e., removing fallen trees and planting new ones) by city professionals occurred quickly, and (b) the aggregation of pixel data into the BGs may lead to a loss of sensitivity when upscaled to a larger area. Regardless, $MSAVI2\Delta$ was found to be relatively more significant compared with other $VI\Delta$ variables. Therefore, it has a

high potential to be used for estimating hurricane debris damage when combined with other indices. As such, it is highly recommended to develop a debris estimation model using $MSAVI2$ and NDBI. They may be utilized in the US Army Corps Engineers model (Equation 1) as vegetation and developed land multipliers.

Finally, aggregating all data into the BGs can be considered as the third caveat of this study, as the target geographical unit in model development is determined subjectively. This allowed us to analyze the debris volume at a relatively finer scale while counting on the socioeconomics; however, the debris collection points provided by the city refers to the stack of debris loaded to a truck, and this stack may consist of the vegetative debris from larger areas. In addition, the accuracy of the sentinel data when aggregated into different geographical units can be tested in a future study to determine the best scale. Nevertheless, the strength of this study lies in the integration of sentinel satellite data and census data to analyze the post-hurricane vegetative debris, and in determining the important variables on post-hurricane debris formation. Additionally, five different vegetation indices were tested to be used in hurricane impact analysis, and $MSAVI2$ performed better than the other VIs.

There are multiple directions for future work and extensions of this study. First, with the availability of debris collection data, the study can be extended to analyze a larger area with more diverse BGs in terms of the hurricane impact, land characteristics, and socioeconomics. Second, vegetation species can be analyzed to identify the most resilient ones to encourage their use in landscaping applications. Third, imagery data from multiple satellites can be combined to obtain cloud-free images with a smaller time gap between the pre- and post-hurricane images, as shown in Thompson et al. (14). This could also help in the analysis of the impact of seasonal vegetation changes on debris formation and remote sensing-based debris assessment. Fourth, one can focus on the seasonal changes between before and after images in more detail. Fifth, robust predictive models can be developed using the proposed framework, which is out of scope for this assessment paper. Finally, the proposed approach, integrated with sentinel and census data, can serve as a useful tool in analyzing socio-ecological injustice and urban sustainability.

Author Contributions

The authors confirm contribution to the paper as follows: study conception and design: AK, MBU, TA, RA, EEO data collection: AK, TA, RA, EEO analysis and interpretation of results: AK, MBU, TA, RA, EEO draft manuscript preparation: AK, MBU, RA, EEO. All authors reviewed the results and approved the final version of the manuscript.


Declaration of Conflicting Interests


The author(s) declared no potential conflicts of interest with respect to the research, authorship, and/or publication of this article.


Funding

The author(s) received no financial support for the research, authorship, and/or publication of this article.

ORCID iDs

Alican Karaer  <https://orcid.org/0000-0002-6704-0379>

Mehmet Baran Ulak  <https://orcid.org/0000-0002-0893-3871>

Reza Arghandeh  <https://orcid.org/0000-0002-0691-5426>

References

- Zhang, F., C. Cao, C. Li, Y. Liu, and D. Huisinsh. A Systematic Review of Recent Developments in Disaster Waste Management. *Journal of Cleaner Production*, Vol. 235, 2019, pp. 822–840. <https://doi.org/10.1016/j.jclepro.2019.06.229>.
- McEntir, D. A. Managing Debris Successfully after Disasters: Considerations and Recommendations for Emergency Managers. *Journal of Emergency Management*, Vol. 4, No. 4, 2006, p. 23. <https://doi.org/10.5055/jem.2006.0039>.
- Horner, M. W., and M. J. Widener. The Effects of Transportation Network Failure on People's Accessibility to Hurricane Disaster Relief Goods: A Modeling Approach and Application to a Florida Case Study. *Natural Hazards*, Vol. 59, No. 3, 2011, pp. 1619–1634. <https://doi.org/10.1007/s11069-011-9855-z>.
- Kocatepe, A., M. B. Ulak, G. Kakareko, E. E. Ozguven, S. Jung, and R. Arghandeh. Measuring the Accessibility of Critical Facilities in the Presence of Hurricane-Related Roadway Closures and an Approach for Predicting Future Roadway Disruptions. *Natural Hazards*, Vol. 95, No. 3, 2019, pp. 615–635. <https://doi.org/10.1007/s11069-018-3507-5>.
- Hu, Z. H., J. B. Sheu, C. Wei, and S. L. Hu. Post-Storm Debris Removal Considering Traffic and Psychological Impacts. *Transportmetrica A: Transport Science*, Vol. 15, No. 2, 2019, pp. 1145–1174. <https://doi.org/10.1080/23249935.2019.1567618>.
- Safapour, E., and S. Kermanshachi. Identification and Categorization of Factors Affecting Duration of Post-Disaster Reconstruction of Interdependent Transportation Systems. *Proc., Construction Research Congress 2020*, Tempe, AZ, No. 10, American Society of Civil Engineers, Reston, VA, 2020, pp. 1290–1299.
- Gaspard, K., M. Martinez, Z. Zhang, and Z. Wu. *Impact of Hurricane Katrina on Roadways in the New Orleans Area*. Technical Assistance Report No. 07–2TA. Louisiana Transportation Research Center, Baton Rouge, 2007.
- Staudhammer, C. L., F. Escobedo, C. Luley, and J. Bond. Patterns of Urban Forest Debris from the 2004 and 2005 Florida Hurricane Seasons. *Southern Journal of Applied Forestry*, Vol. 33, No. 4, 2009, pp. 193–196. <https://doi.org/10.1093/sjaf/33.4.193>.
- FEMA. FEMA Approves Additional \$46.8 Million for FDOT Hurricane Michael Debris Removal Expenses. <https://www.fema.gov/press-release/20210318/fema-approves-additional-468-million-fdot-hurricane-michael-debris-removal>. Accessed May 4, 2021.
- Duryea, M. L., E. Kampf, R. C. Littell, and C. D. Rodriguez-Pedraza. Hurricanes and the Urban Forest: I. Effects on Southeastern United States Coastal Plain Tree Species. *Arboriculture and Urban Forestry*, Vol. 33, No. 2, 2007, pp. 98–112.
- Duryea, M. L., E. Kampf, R. C. Littell, and C. D. Rodriguez-Pedraza. Hurricanes and the Urban Forest: II. Effects on Tropical and Subtropical Tree Species. *Arboriculture and Urban Forestry*, Vol. 33, No. 2, 2007, pp. 98–112.
- Escobedo, F. J., C. J. Luley, J. Bond, C. Staudhammer, and C. Bartel. Hurricane Debris and Damage Assessment for Florida Urban Forests. *Arboriculture and Urban Forestry*, Vol. 35, No. 2, 2009, pp. 100–106.
- Thompson, B., F. J. Escobedo, C. L. Staudhammer, J. Bond, and C. Luley. *Urban Forests in Florida: Storm Damage Assessment Utility for Estimating Hurricane-Caused Tree Debris*. University of Florida, Institute of Food and Agricultural Sciences, FOR268. 2010.
- Thompson, B. K., F. J. Escobedo, C. L. Staudhammer, C. J. Matyas, and Y. Qiu. Modeling Hurricane-Caused Urban Forest Debris in Houston, Texas. *Landscape and Urban Planning*, Vol. 101, No. 3, 2011, pp. 286–297. <https://doi.org/10.1016/j.landurbplan.2011.02.034>.
- Wyman, M., F. Escobedo, T. Stein, M. Orfanedes, and R. Northrop. Community Leader Perceptions and Attitudes toward Coastal Urban Forests and Hurricanes in Florida. *Southern Journal of Applied Forestry*, Vol. 36, No. 3, 2012, pp. 152–158. <https://doi.org/10.5849/sjaf.10-022>.
- U.S. Army Corps of Engineers. *Debris Management Guide, APPENDIX A: Hurricane Debris Estimation Model*. USACE, Washington, D.C., 2008.
- Federal Emergency Management Agency. *Debris Estimating Field Guide*. Publication FEMA 329. FEMA, Washington, D.C., 2010.
- Umpierre, D., and G. Margoles. Broward County's Web-Based Hurricane Debris Estimation Tool (HurDET). *2005 ESRI International User Conference Proceedings*, 2005.
- Szantoi, Z., S. Malone, F. Escobedo, O. Misas, S. Smith, and B. Dewitt. A Tool for Rapid Post-Hurricane Urban Tree Debris Estimates Using High Resolution Aerial Imagery. *International Journal of Applied Earth Observation and Geoinformation*, Vol. 18, No. 1, 2012, pp. 548–556. <https://doi.org/10.1016/j.jag.2011.10.009>.
- Hoque, M. A. A., S. Phinn, C. Roelfsema, and I. Childs. Assessing Tropical Cyclone Impacts Using Object-Based Moderate Spatial Resolution Image Analysis: A Case Study in Bangladesh. *International Journal of Remote Sensing*, Vol. 37, No. 22, 2016, pp. 5320–5343. <https://doi.org/10.1080/01431161.2016.1239286>.
- Hu, T., and R. B. Smith. The Impact of Hurricane Maria on the Vegetation of Dominica and Puerto Rico Using

- Multispectral Remote Sensing. *Remote Sensing*, Vol. 10, No. 6, 2018, p. 827. <https://doi.org/10.3390/rs10060827>.
22. Hoque, M. A. A., S. Phinn, C. Roelfsema, and I. Childs. Tropical Cyclone Disaster Management Using Remote Sensing and Spatial Analysis: A Review. *International Journal of Disaster Risk Reduction*, Vol. 22, 2017, pp. 345–354. <https://doi.org/10.1016/j.ijdrr.2017.02.008>.
 23. Metternicht, G. Vegetation Indices Derived from High-Resolution Airborne Videography for Precision Crop Management. *International Journal of Remote Sensing*, Vol. 24, No. 14, 2003, pp. 2855–2877. <https://doi.org/10.1080/01431160210163074>.
 24. Zha, Y., J. Gao, and S. Ni. Use of Normalized Difference Built-up Index in Automatically Mapping Urban Areas from TM Imagery. *International Journal of Remote Sensing*, Vol. 24, No. 3, 2003, pp. 583–594. <https://doi.org/10.1080/01431160304987>.
 25. Tang, Z., Y. Li, Y. Gu, W. Jiang, Y. Xue, Q. Hu, T. LaGrange, A. Bishop, J. Drahotka, and R. Li. Assessing Nebraska Playa Wetland Inundation Status during 1985–2015 Using Landsat Data and Google Earth Engine. *Environmental Monitoring and Assessment*, Vol. 188, No. 12, 2016, pp. 1–14. <https://doi.org/10.1007/s10661-016-5664-x>.
 26. Ghorbanzadeh, M., M. Koloushani, M. B. Ulak, E. E. Ozguven, and R. A. Jouneghani. Statistical and Spatial Analysis of Hurricane-Induced Roadway Closures and Power Outages. *Energies*, Vol. 13, No. 5, 2020, p. 1098. <https://doi.org/10.3390/en13051098>.
 27. Ulak, M. B., A. Kocatepe, L. M. Konila Sriram, E. E. Ozguven, and R. Arghandeh. Assessment of the Hurricane-Induced Power Outages from a Demographic, Socioeconomic, and Transportation Perspective. *Natural Hazards*, Vol. 92, No. 3, 2018, pp. 1489–1508. <https://doi.org/10.1007/s11069-018-3260-9>.
 28. Chen, M., A. Karaer, E. E. Ozguven, T. Abichou, R. Arghandeh, and J. Nienhuis. Developing City-Wide Hurricane Impact Maps Using Real-Life Data on Infrastructure, Vegetation and Weather. *Transportation Research Record: Journal of the Transportation Research Board*, 2021. 2675: 393–404.
 29. Faturechi, R., and E. Miller-Hooks. Travel Time Resilience of Roadway Networks under Disaster. *Transportation Research Part B: Methodological*, Vol. 70, 2014, pp. 47–64. <https://doi.org/10.1016/j.trb.2014.08.007>.
 30. Larsen, T., K. Porter, M. Zadeh, C. Van Anne, and C. Scawthorn. *Impact of Hurricane Andrew on Performance Interaction and Recovery of Lifelines*. National Science Foundation. Grant BCS-9224819. 1996.
 31. Demirogluk, S., and K. Ozbay. Bayesian Spatial Modeling and Risk Mapping of Downed Trees along the Roadways Using Data from Hurricanes Irene and Sandy. Presented at 94th Annual Meeting of the Transportation Research Board, Washington, D.C., 2015.
 32. Davidson, R. A., H. Liu, I. K. Sarpong, P. Sparks, and D. V. Rosowsky. Electric Power Distribution System Performance in Carolina Hurricanes. *Natural Hazards Review*, Vol. 4, No. 1, 2003, pp. 36–45. [https://doi.org/10.1061/\(asce\)1527-6988\(2003\)4:1\(36\)](https://doi.org/10.1061/(asce)1527-6988(2003)4:1(36)).
 33. Vijayan, L., W. Huang, K. Yin, E. Ozguven, S. Burns, and M. Ghorbanzadeh. Evaluation of Parametric Wind Models for More Accurate Modeling of Storm Surge: A Case Study of Hurricane Michael. *Natural Hazards*, Vol. 106, No. 3, 2021, pp. 2003–2024. <https://doi.org/10.1007/s11069-021-04525-y>.
 34. McRoberts, D. B., S. M. Quiring, and S. D. Guikema. Improving Hurricane Power Outage Prediction Models Through the Inclusion of Local Environmental Factors. *Risk Analysis*, Vol. 38, No. 12, 2018, pp. 2722–2737. <https://doi.org/10.1111/risa.12728>.
 35. Ulak, M. B., A. Yazici, and E. E. Ozguven. A Prescriptive Model to Assess the Socio-Demographics Impacts of Resilience Improvements on Power Networks. *International Journal of Disaster Risk Reduction*, Vol. 51, 2020, p. 101777. <https://doi.org/10.1016/j.ijdrr.2020.101777>.
 36. Gabe, T., G. Falk, M. McCarty, and V. W. Mason. *Hurricane Katrina: Social-Demographic Characteristics of Impacted Areas*. Publication CRS-RL33141. Congressional Research Service, Library of Congress, Washington, D.C., 2005.
 37. Bjarnadottir, S., Y. Li, and M. G. Stewart. Social Vulnerability Index for Coastal Communities at Risk to Hurricane Hazard and a Changing Climate. *Natural Hazards*, Vol. 59, No. 2, 2011, pp. 1055–1075. <https://doi.org/10.1007/s11069-011-9817-5>.
 38. Lindell, M. K., and C. S. Prater. Assessing Community Impacts of Natural Disasters. *Natural Hazards Review*, Vol. 4, No. 4, 2003, pp. 176–185. [https://doi.org/10.1061/\(asce\)1527-6988\(2003\)4:4\(176\)](https://doi.org/10.1061/(asce)1527-6988(2003)4:4(176)).
 39. Chakalian, P. M., L. C. Kurtz, and D. M. Hondula. After the Lights Go Out: Household Resilience to Electrical Grid Failure Following Hurricane Irma. *Natural Hazards Review*, Vol. 20, No. 4, 2019, p. 05019001. [https://doi.org/10.1061/\(asce\)nh.1527-6996.0000335](https://doi.org/10.1061/(asce)nh.1527-6996.0000335).
 40. Gazzea, M., A. Karaer, N. Balafkan, E. E. Ozguven, and R. Arghandeh. *Post-Hurricanes Roadway Closure Detection Using Satellite Imagery and Semi-Supervised Ensemble Learning*. Presented at 100th Annual Meeting of the Transportation Research Board, Washington, D.C., 2021, No. TRBAM-21-00892.
 41. Gazzea, M., A. Karaer, M. Ghorbanzadeh, N. Balafkan, T. Abichou, E. E. Ozguven, and R. Arghandeh. Automated Satellite-Based Assessment of Hurricane Impacts on Roadways. *IEEE Transactions on Industrial Informatics*, 2021. <https://doi.org/10.1109/TII.2021.3082906>.
 42. Karaer, A., M. B. Ulak, T. Abichou, R. Arghandeh, and E. E. Ozguven. Leveraging Remote Sensing Indices for Hurricane-Induced Vegetative Debris Assessment: A GIS-Based Case Study for Hurricane Michael. Presented at 100th Annual Meeting of the Transportation Research Board, Washington, D.C., 2021, No. TRBAM-21-04450.
 43. Chuvieco, E., M. P. Martín, and A. Palacios. Assessment of Different Spectral Indices in the Red-Near-Infrared Spectral Domain for Burned Land Discrimination. *International Journal of Remote Sensing*, Vol. 23, No. 23, 2002, pp. 5103–5110. <https://doi.org/10.1080/01431160210153129>.
 44. Zhang, X. K., X. Zhang, Q. Q. Lan, and M. H. Ali Baig. Automated Detection of Coastline Using Landsat TM Based on Water Index and Edge Detection Methods. *Proc.*,

- 2nd International Workshop on Earth Observation and Remote Sensing Applications, EORSA 2012, Shanghai, China, IEEE, New York, 2012, pp. 153–156.
45. Purevdorj, T. S., R. Tateishi, T. Ishiyama, and Y. Honda. Relationships between Percent Vegetation Cover and Vegetation Indices. *International Journal of Remote Sensing*, Vol. 19, No. 18, 1998, pp. 3519–3535. <https://doi.org/10.1080/014311698213795>.
 46. Xue, J., and B. Su. Significant Remote Sensing Vegetation Indices: A Review of Developments and Applications. *Journal of Sensors*, Vol. 2017, 2017, pp. 1–17. <https://doi.org/10.1155/2017/1353691>.
 47. Ramsey, E. W., D. K. Chappell, and D. G. Baldwin. AVHRR Imagery Used to Identify Hurricane Damage in a Forested Wetland of Louisiana. *Photogrammetric Engineering and Remote Sensing*, Vol. 63, No. 3, 1997, pp. 293–297.
 48. Rodgers, J. C., A. W. Murrah, and W. H. Cooke. The Impact of Hurricane Katrina on the Coastal Vegetation of the Weeks Bay Reserve, Alabama from NDVI Data. *Estuaries and Coasts*, Vol. 32, No. 3, 2009, pp. 496–507. <https://doi.org/10.1007/s12237-009-9138-z>.
 49. Qi, J., A. Chehbouni, A. R. Huete, Y. H. Kerr, and S. Soroshian. A Modify Soil Adjust Vegetation Index. *Remote Sensing of Environment*, Vol. 126, 1994, pp. 119–126.
 50. Rouse, J. W., R. H. Hass, J. A. Schell, and D. W. Deering. Monitoring Vegetation Systems in the Great Plains with ERTS. *Proc., Third Earth Resources Technology Satellite (ERTS) Symposium*, Washington, D.C., Vol. 1, Science and Technical Information Office, NASA, Washington, D.C., 1973, pp. 309–317.
 51. Wikipedia. Normalized Difference Vegetation Index (NDVI). https://en.wikipedia.org/wiki/Normalized_difference_vegetation_index#cite_note-1. Accessed June 10, 2020.
 52. National Aeronautics and Space Administration. *Measuring Vegetation (NVDI & EVI)*. NASA Earth Observatory, Washington, D.C., 2000.
 53. Buschmann, C., and E. Nagel. In Vivo Spectroscopy and Internal Optics of Leaves as Basis for Remote Sensing of Vegetation. *International Journal of Remote Sensing*, Vol. 14, No. 4, 1993, pp. 711–722. <https://doi.org/10.1080/01431169308904370>.
 54. Qi, J., Y. Kerr, and A. Chehbouni. External Factor Consideration in Vegetation Index Development. *Proc., 6th International Symposium on Physical Measurements and Signatures in Remote Sensing*, Val d'Isere, France, 1994, CNES, pp. 723–730.
 55. Huete, A. R. A Soil-Adjusted Vegetation Index (SAVI). *Remote Sensing of Environment*, Vol. 25, No. 3, 1988, pp. 295–309. [https://doi.org/10.1016/0034-4257\(88\)90106-X](https://doi.org/10.1016/0034-4257(88)90106-X).
 56. Chen, Y. Correlation of Saltbush Cover Measurements to TM Wavebands and Vegetation Indices. *International Geoscience and Remote Sensing Symposium (IGARSS)*, Vol. 5, 1999, pp. 2590–2592. <https://doi.org/10.1109/igarss.1999.771586>.
 57. Liu, A., J. Wang, Z. Liu, and J. Wang. Monitoring Desertification in Arid and Semi-Arid Areas of China with NOAA-AVHRR and MODIS Data. *International Geoscience and Remote Sensing Symposium (IGARSS)*, Vol. 4, 2005, pp. 2362–2364. <https://doi.org/10.1109/IGARSS.2005.1525451>.
 58. Phillips, R., O. Beerli, E. Scholljegerdes, D. Bjergaard, and J. Hendrickson. Integration of Geospatial and Cattle Nutrition Information to Estimate Paddock Grazing Capacity in Northern US Prairie. *Agricultural Systems*, Vol. 100, No. 1–3, 2009, pp. 72–79. <https://doi.org/10.1016/j.agsy.2009.01.002>.
 59. USDA. The Landscape Toolbox. <https://wiki.landscape-toolbox.org/doku.php>. Accessed June 8, 2020.
 60. Haboudane, D., J. R. Miller, E. Pattey, P. J. Zarco-Tejada, and I. B. Strachan. Hyperspectral Vegetation Indices and Novel Algorithms for Predicting Green LAI of Crop Canopies: Modeling and Validation in the Context of Precision Agriculture. *Remote Sensing of Environment*, Vol. 90, No. 3, 2004, pp. 337–352. <https://doi.org/10.1016/j.rse.2003.12.013>.
 61. ENVI. Narrowband Greenness. <https://www.harrisgeospatial.com/docs/NarrowbandGreenness.html>. Accessed June 10, 2020.
 62. Gitelson, A. A., R. Stark, U. Grits, D. Rundquist, Y. Kaufman, and D. Derry. Vegetation and Soil Lines in Visible Spectral Space: A Concept and Technique for Remote Estimation of Vegetation Fraction. *International Journal of Remote Sensing*, Vol. 23, No. 13, 2002, pp. 2537–2562. <https://doi.org/10.1080/01431160110107806>.
 63. ESRI. Use Deep Learning to Assess Palm Tree Health. 2020. <https://learn.arcgis.com/en/projects/use-deep-learning-to-assess-palm-tree-health/#estimate-vegetation-health>. Accessed November 30, 2020.
 64. Xu, H. Modification of Normalised Difference Water Index (NDWI) to Enhance Open Water Features in Remotely Sensed Imagery. *International Journal of Remote Sensing*, Vol. 27, No. 14, 2006, pp. 3025–3033. <https://doi.org/10.1080/01431160600589179>.
 65. McFeeters, S. K. The Use of the Normalized Difference Water Index (NDWI) in the Delineation of Open Water Features. *International Journal of Remote Sensing*, Vol. 17, No. 7, 1996, pp. 1425–1432. <https://doi.org/10.1080/01431169608948714>.
 66. Stanturf, J. A., S. L. Goodrick, and K. W. Outcalt. Disturbance and Coastal Forests: A Strategic Approach to Forest Management in Hurricane Impact Zones. *Forest Ecology and Management*, Vol. 250, No. 1–2, 2007, pp. 119–135. <https://doi.org/10.1016/j.foreco.2007.03.015>.
 67. Data Commons. Tallahassee Demographics. *Place Explorer*. <https://datacommons.org/place/geoId/1270600?topic=Demographics>. Accessed April 19, 2021.
 68. Data Commons. Tallahassee Education. *Place Explorer*. <https://datacommons.org/place/geoId/1270600?topic=Education>. Accessed April 19, 2021.
 69. City of Tallahassee. Urban Forest Master Plan Goals & Progress. <https://www.talgov.com/place/pln-urbanforestry2.aspx>. Accessed December 1, 2020.
 70. Leon Trees. Explore Our Sense of Place. <http://leontrees.org/explore/>. Accessed December 1, 2020.

71. City of Tallahassee – Leon County. TlCGIS Data. <https://geodata-tlcfgis.opendata.arcgis.com/>. Accessed June 10, 2020.
72. NOAA. Saffir-Simpson Hurricane Wind Scale. <https://www.nhc.noaa.gov/aboutshws.php>. Accessed June 9, 2020.
73. Wikipedia. Saffir–Simpson Scale. https://en.wikipedia.org/wiki/Saffir–Simpson_scale. Accessed June 9, 2020.
74. NOAA National Centers for Environmental Information. State of the Climate: Tropical Cyclones for Annual 2018. <https://www.ncdc.noaa.gov/sotc/tropical-cyclones/201108>. Accessed January 19, 2021.
75. Wikipedia. Hurricane Michael. https://en.wikipedia.org/wiki/Hurricane_Michael. Accessed May 21, 2020.
76. United States Census Bureau. American Community Survey (ACS). <https://www.census.gov/acs/www/data/datatables-and-tools/data-profiles/>. Accessed July 31, 2020.
77. FDOT. FGDL Metadata Explorer. <https://www.fgdl.org/metadataexplorer/explorer.jsp>. Accessed June 9, 2020.
78. Kalantari, Z., C. S. S. Ferreira, A. J. Koutsouris, A.-K. Ahlmer, A. Cerdà, and G. Destouni. Assessing Flood Probability for Transportation Infrastructure Based on Catchment Characteristics, Sediment Connectivity and Remotely Sensed Soil Moisture. *Science of The Total Environment*, Vol. 661, 2019, pp. 393–406. <https://doi.org/10.1016/j.scitotenv.2019.01.009>.
79. Karaer, A., N. Balafkan, M. Gazzea, R. Arghandeh, and E. E. Ozguven. Analyzing COVID-19 Impacts on Vehicle Travels and Daily Nitrogen Dioxide (NO₂) Levels among Florida Counties. *Energies*, Vol. 13, No. 22, 2020, p. 6044. <https://doi.org/10.3390/en13226044>.
80. ESA. Copernicus Open Access Hub. <https://scihub.copernicus.eu/dhus/#/home>. Accessed June 9, 2020.
81. Wikipedia. Sentinel-2. <https://en.wikipedia.org/wiki/Sentinel-2>. Accessed June 22, 2020.
82. Wikipedia. Pearson Correlation Coefficient. [https://en.wikipedia.org/wiki/Pearson_correlation_coefficient#:~:text=Instatistics%2C the Pearson correlation,two variables X and Y](https://en.wikipedia.org/wiki/Pearson_correlation_coefficient#:~:text=Instatistics%2C%20the%20Pearson%20correlation,two%20variables%20X%20and%20Y.). Accessed June 15, 2020.
83. Esri. How Exploratory Regression Works. <https://pro.arcgis.com/en/pro-app/tool-reference/spatial-statistics/how-exploratory-regression-works.htm>. Accessed December 1, 2020.
84. Lai, F., and X. Yang. Integrating Spectral and Non-Spectral Data to Improve Urban Settlement Mapping in a Large Latin-American City. *GIScience & Remote Sensing*, Vol. 57, No. 6, 2020, pp. 830–844. <https://doi.org/10.1080/15481603.2020.1814032>.